Emerging investigator series: photocatalysis for MBR effluent post-treatment: assessing the effects of effluent organic matter characteristics

Mostafa Maghsoodi, Céline Jacquin, Benoit Teychené, Marc Heran, Volodymyr Tarabara, Geoffroy Lesage, Samuel Snow

Title: Photocatalysis for MBR Effluent Post-Treatment: Assessing the Effects of Effluent Organic Matter Characteristics

Authors:

Mostafa Maghsoodi[1T], Céline Jacquin[2T], Benoit Teychené[3], Marc Heran[2], Volodymyr V. Tarabara[4], Geoffroy Lesage[*2], Samuel D. Snow[*1]

[1]Department of Civil and Environmental Engineering, Louisiana State University, 3255 Patrick Taylor Hall, Baton Rouge, Louisiana 70803, United States.

[2]IEM (Institut Européen des Membranes), UMR 5635 (CNRS-ENSCM-UM), Université de Montpellier, Place E. Bataillon, F- 34095, Montpellier, France.

[3]Institut de Chimie des Milieux et Matériaux de Poitiers (IC2MP – UMR CNRS 7285), Université de Poitiers, Ecole Nationale Supérieure d'Ingénieurs de Poitiers, 7 rue Marcel Doré, Bâtiment 16, TSA 41105, 86073 Poitiers Cedex 9, France.

[4]Department of Civil and Environmental Engineering, Michigan State University, 428 S. Shaw Lane, East Lansing, Michigan 48824, United States.

[T]These authors contributed equally.

*Corresponding authors: SSnow@lsu.edu; Geoffroy.Lesage@umontpellier.fr;

Abstract: Dissolved organic matter (DOM) poses a serious challenge to applied photocatalysis. Membranes may offer a promising synergistic opportunity to enable efficient photocatalysts in the presence of DOM. Membrane bioreactor (MBR) effluent from a municipal treatment plant was studied to elucidate the effects of filtration and organic matter composition on photocatalysis. Effluent samples were collected from MBR units during routine operation and before/after chemical cleaning. Additional DOM samples from the bulk supernatant were separated into colloidal, hydrophobic and transphilic fractions, providing a novel examination of the inhibition potential of DOM. These DOM fractions and the effluent organic matter (EfOM) samples were then characterized utilizing three-dimensional excitation–emission matrix (3DEEM) fluorescence spectroscopy and assayed for their potential to inhibit TiO_2-mediated photocatalytic degradation of a probe compound, *para*-chlorobenzoic acid (*p*CBA). The colloidal fraction of DOM was found to exert the strongest

inhibition, followed by the transphilic, then the hydrophobic fractions; at 5 mgC/L, these fractions reduced the photodegradation rates by approximately 75%, 27%, and 17%, respectively. Of the effluent samples, EfOM from the recently-cleaned membrane caused the greatest inhibition of photocatalysis (~100% reduction at 0.5 to 2.0 mgC/L), whereas the effluent from the fouled membrane provided the least inhibition (~33% reduction at 2.0 mgC/L). The 3DEEM analysis predicted inhibitory action of both DOM and EfOM, based on total fluorescence volumes. Results here demonstrate the prospective utility of combining membrane technologies with photocatalytic processes.

1. Introduction

As the human population continues to grow, careful utilization of natural resources becomes increasingly more important. Water usage, and particularly reuse, is a critical topic for many communities.[1, 2] The development of membrane bioreactor (MBR) technology has been an important step towards wastewater reuse, given substantial advantages over conventional activated sludge systems in terms of improved efficiency and effluent quality.[3] Despite these benefits that stem from the use a physical barrier (membranes), several types of contaminants can pass through the membranes and pose significant health risks upon release of the effluent into the environment. Indeed, viruses have been found in the effluents of state-of-the-art MBR treatment plants.[4, 5] In addition, pharmaceuticals[6, 7] and, more recently, antibiotic resistant genes have drawn attention as significant concerns posing environmental and health risks.[8] Thus, MBR systems require a disinfection step post-filtration to provide a safeguard. Although UV disinfection can be used in lieu of chlorination, and thereby avoid the necessity for an added dechlorination step, there are disadvantages: UV treatment does not significantly degrade antibiotic resistant genes[8] and many pollutants are recalcitrant to UV at commonly applied UV doses.[9]

Given these post-filtration challenges, an integration of innovative technologies could provide the key functionality to eliminate the remaining hazards from MBR effluent. In particular, photocatalytic materials applied in conjunction with existing UV dosing systems could produce reactive oxygen to

destroy these contaminants via advanced oxidation processes.[9-12] Germicidal UV radiation, a subset of the spectrum of short-wavelength UV light, often called UVC,[13, 14] can be enhanced by the addition of photocatalytic processes to promote the production of reactive oxygen species (ROS). These ROS are known to be particularly effective at inactivating viruses compared to bacteria which have protective cell membranes.[15-18] For example, the inactivation kinetics *Escherichia coli* by hydroxyl radicals (·OH) or by singlet oxygen ($^1O_2$) have been shown to have a lag-phase where the cell membrane protects the bacteria's intracellular components against ROS attack,[15, 16, 18] whereas the genetic and essential components of viruses, such as MS2 bacteriophage, have very little protection and therefore no delay in their inactivation kinetics.[15, 16]A combined UVC-photocatalytic system is a plausible conception that could serve as an advanced oxidation process to oxidize pharmaceutical compounds in addition to providing disinfection activity.[10]

Application of photocatalytic processes to natural or waste waters faces a significant challenge in the form of non-target organic matter interferences. In the case of MBRs, effluent organic matter (EfOM) contains a variety of molecules that are known to quench hydroxyl radicals (·OH),[19] which are generally the most important ROS in any advanced oxidation—including TiO_2 mediated photocatalysis. MBR EfOM is a complex mixture of organic molecules such as proteins, polysaccharides, humic substances and nucleic acids.[20-23] These molecules originate primarily from microbial activity (soluble microbial products, SMPs), produced during secondary biological treatment (via suspended or attached growth processes) , and are typically found at concentrations ranging from 3 to 25 mgC/L.[21, 22, 24-27] EfOM can interfere with photocatalytic treatment through different inhibitory mechanisms. First, EfOM absorbs significant amounts of UV light, limiting the amount of photons available for catalyst excitation.[28] Second, EfOM quenches ROS, preventing reactions with the target compounds or microorganisms.[29, 30] This competition for ROS between the non-target EfOM and the target constituents can occur in two ways: scavenging of surface-bound ROS by EfOM and quenching of bulk phase ROS.[15, 29, 31, 32] Within the complex mixture of EfOM, less than 2% of the dissolved and colloidal organic materials are considered target contaminants, such as viruses or pharmaceuticals that originate from the influent wastewater;[33] thus, most photocatalytically generated ·OH radicals will be

quenched by reactions with non-target EfOM. Indeed, EfOM has been reported to scavenge between 65 and 95% of ·OH in conventional effluents and is considered the most important ·OH-scavenger in such systems.[34, 35] EfOM constituents, such as fulvic acid and humic acid (HA), have a net negative charge above pH 3 due to the presence of phenolic and carboxylic groups.[36, 37] These molecules can therefore interact favorably with and adsorb onto the polar surface of TiO_2, reacting directly with ROS production sites.

It is important to understand the factors that control surface and bulk quenching mechanisms; ROS-EfOM reactivity and EfOM-photocatalyst adsorption affinities drive bulk and surface quenching routes, respectively. Different ROS have differential reactivities; for example, singlet oxygen ($^1O_2$) is less reactive and more selective than ·OH.[38] Likewise, EfOM constituents may also vary in propensity to react with ROS, with some compounds being recalcitrant to strong oxidants, while others readily react with weaker ROS, such as $^1O_2$.[30, 39] With regard to adsorption interactions, the nature of the photocatalyst surface will determine the type of EfOM molecules that will adsorb onto the photocatalyst surface. These types of interactions have been studied in depth for the case of membrane fouling by organic matter,[40-42] and offer potential insights into DOM-photocatalyst interactions.

Membrane technology can be used to selectively remove fractions of organic matter. In the case of an MBR treating municipal wastewater, the membrane's material, pore size, and fouling state affect its selectivity and, therefore, the composition of the EfOM.[43] It is known that, in general, hydrophilic macromolecular and colloidal portions of organic matter cause more reversible membrane fouling than other fractions in MBR systems by forming a cake layer.[41, 44, 45] Fouling changes the effective pore size and surface characteristics of membranes; consequently, permeate quality changes over the operational timeline, since the last chemical cleaning event.[46-48] Membrane operation may control DOM retention and thereby the composition of DOM that passes through (EfOM); therefore, the time since last cleaning event could be an important parameter when considering the use of effluent disinfection strategies. The extent to which membrane operation time can be used as a control EfOM quality is not well known. A better understanding of the variability of EfOM constituents as a function of membrane operational parameters is critical for applying post-filtration disinfection technologies. Elucidating the

effects of membrane operation on EfOM content provides an excellent opportunity to scrutinize the effects of EfOM constituents on photocatalytic processes, a significant area of need for the field of photocatalytic water treatment.

While TiO_2 systems have been studied extensively, the mechanisms driving ROS inhibition by DOM are poorly understood. A recent literature review quantified the number of research articles investigating "photocatalysis" and "natural organic matter" and found that of the 17,500 papers found when searching for photocatalysis, only 0.8% (137) also referenced DOM.[49] The segregation of DOM into fractions to discern phenomenological effects of constituents on photocatalytic processes is therefore a critical step towards practical application of photocatalysts. A study completed in 2014 on the effects of size-fractionation of DOM on the photocatalytic degradation of DOM by TiO_2 is perhaps the first report to scrutinize the inhibitory mechanism by analyzing fractionated DOM samples.[50] The approach in the present study utilizes EfOM from differentially fouled bioreactor membranes and functionally fractionated bioreactor DOM to provide a novel assessment of inhibitory mechanisms of DOM in TiO_2 photocatalysis.

Bulk supernatant DOM and EfOM samples collected in 2015 and 2016 from an operational MBR in a municipal wastewater treatment plant (WWTP) are studied here. Fractionation of samples in terms of DOM size and hydrophobicity, a method commonly used to isolate organics, was applied to MBR bulk supernatant. Here, the effects of different fractions of bulk supernatant DOM and EfOM samples on photocatalytic processes are assessed to identify the most important fractions to reject during filtration. Three-dimensional fluorescence excitation-emission matrix (3DEEM) analysis is employed to characterize the resultant DOM from fractionation procedures and the MBR effluent samples, to better forecast and understand their effect on photocatalysis processes. 3DEEM is increasingly employed to understand DOM evolution in wastewater systems.[51, 52] A recent study also highlighted that 3DEEM can be used to distinguish proteins from biopolymers and humic substances and to quantify building blocks, with potential use as an on-line indicator to describe DOM fate and behavior.[53] Further, this technique has distinguished the effects of different types of DOM on water treatment technologies (i.e., membrane fouling, UV attenuation, and disinfection byproduct

formation).[43, 54-56] Inhibitory profiles of the DOM fractions and EfOM samples are established by measuring the photodegradation of a molecular probe as a function of total organic carbon (TOC) concentration. Inhibition mechanisms are discussed in the context of an experimentally validated model that accounts for surface and bulk phase quenching processes simultaneously.[29] Finally, comments are made on the prospective utility of photocatalytic membrane reactors (PMRs)[57-59] as a combined treatment process.

2. Materials and methods

2.1. Chemicals

Humic acid and 4-chlorobenzoic acid were obtained from Alfa Aesar (Haverhill, MA). Titanium dioxide (99.9% Anatase) was purchased from Alfa Aesar with a nominal particle size of 32 nm and surface area of 45 m^2/g. Ultrapure water (>18.2 MΩ-cm) was produced using a Nanopure Infinity system (Thermo Fisher Scientific Inc., Waltham, MA). HPLC solvents were HPLC-grade and obtained from Alfa Aesar.

2.2. EfOM sampling

EfOM samples were collected from a full-scale MBR wastewater treatment plant (La Grande Motte, France), which treats municipal wastewater and serves a population of approximately 60,000. The plant performs biological removal of nitrogen (nitrification and denitrification) and phosphorus. The plant comprises four MBR tanks, each equipped with KUBOTA Submerged Membrane Units® (SMUs, KUBOTA, Japan), which are flat sheet microporous membranes made of chlorinated polyethylene with an average pore size of 0.2 μm and a nominal pore size of 0.4 μm. Only two MBR tanks were studied. Here we define MBR1 as the unit which underwent chemical cleaning and MBR2 as a reference unit that did not undergo chemical cleaning during the sampling period. MBR2 was two months into a three- to four-month cycle and therefore was chosen to represent a membrane during normal operation. To assess the cleaning effect, activated sludge (AS) and permeate samples were taken from MBR1 and MBR2 one day before and one day after the cleaning procedure took place for

MBR1 (June 2016). After sampling, AS samples were filtered with a 1.2 µm glass microfiber filters (Whatman GF/C) to collect the dissolved portion of the AS, labeled as the bulk supernatant (BSN). Hence, four samples from the MBR1 cleaning campaign and two samples from MBR2 were collected and analyzed for this study: and each sample was given a reference name as shown in Table 1.

In addition to the samples taken to assess the effects of membrane cleaning, 500 L of AS were also collected from MBR1 in June 2015 to perform DOM fractionation using dialysis and XAD-resins. Prior to fractionation the AS was filtered successively through 50 µm and 2 µm polypropylene filters to collect BSN. Next, softening was performed using a sodium cation-exchange resin (Purolite, France) to remove calcium and magnesium ions, to avoid ion complexation with DOM and scaling during the following step: reverse osmosis (RO).[60] DOM in the BSN sample was concentrated via RO in order to minimize the time required for the fractionation step. A Filmtec TW 30 membrane was used for the RO process, since it is known to be more resistant to DOM adsorption.[61] The RO process effectively concentrated the BSN by 100-fold which was subsequently used to perform DOM fractionation.

2.3. DOM fractionation

The first fractionation step consisted of isolating the colloidal portion of DOM by size exclusion, using dialysis (3.5 kDa, Spectra/Por 6 Dialysis Membrane) against HCl (0.01 mol/L, pH 2). Next, organic colloids were separated from colloidal silica and precipitated salts by dialysis (3.5 kDa) against 0.2 mol/L HF.[62] The dialysate, approximately 30 L of HCl solution containing DOM compounds with a molecular weight smaller than 3.5 kDa, was then passed through XAD8 and XAD4 resins (Amberlite, Sigma Aldrich) arranged in tandem. This step allowed for the collection of hydrophobic (HPO) and transphilic (TPI) fractions.[42, 63] The hydrophilic (HPI) fraction, composed of low molecular weight hydrophilic DOM and salts, was collected in the outlet of the resins tandem. This fraction, however, was not used in the study because the solution contained highly concentrated salts, which co-precipitate with the organic matter. Removing these salts, while possible, would have required a complex purification step called azeotrophic distillation.[64] To collect HPO and TPI fractions adsorbed

onto XAD resins, elution with an acetonitrile/MQ water solution (75/25% v/v) was performed, followed by evaporation and freeze-drying of the respective organic matter samples.

Table 1. Nomenclature of samples and fractions based on their respective MBR units, sampling period, or fractionation procedure.

Label	Collection	Description
BSNf-MBR1	MBR1, Bulk Supernatant	Fouled membrane (Pre-wash)
BSNw-MBR1	MBR1, Bulk Supernatant	Washed membrane (Post-wash)
BSN-MBR2	MBR2, Bulk Supernatant	Midpoint between chemical cleaning events
Pf-MBR1	MBR1, Permeate	Fouled membrane (Pre-wash)
Pw-MBR1	MBR1, Permeate	Washed membrane (Post-wash)
P-MBR2	MBR2, Permeate	Midpoint between chemical cleaning events
C	MBR1, Bulk Supernatant	Colloidal fraction
HPO	MBR1, Bulk Supernatant	Hydrophobic fraction
TPI	MBR1, Bulk Supernatant	Transphilic fraction

2.4. DOM characterization

2.4.1 TOC and UV_{254} absorbance measurements

TOC analysis was performed using a TOC-VCSH Shimadzu analyzer (Shimadzu Japan). The UV_{254} absorbance was measured in a 1 cm quartz cuvette using a UV-VIS spectrophotometer (UV-2401PC, Shimadzu, Japan). The specific UV absorbance ($SUVA_{254}$) was then calculated as the ratio of UV_{254} absorbance and TOC value.[65] These analyses are reported in Table S1.

2.4.2. 3DEEM analysis

Fluorescence spectra were obtained using a Perkin-Elmer LS-55 spectrometer (USA) and a procedure described elsewhere.[53] Spectra were divided into five regions as defined by Chen et al.,[54] corresponding to different groups of fluorophores. The regions were categorized by excitation-emission ranges, as noted in Table 2. Region I is associated with aromatic protein-like fluorophores type I (tyrosine type); Region II is associated to aromatic protein-like fluorophores type II (tyrosine type); Region III corresponds to fulvic acid-like fluorophores; and Region IV and V are associated with SMP-like fluorophores tryptophane type) and humic acid-like fluorophores, respectively.

Table 2. Excitation and emission wavelength classifications of fluorophores.

	Region I	Region II	Region III	Region IV	Region V
Excitation, nm	200 – 250			250 – 350	250 – 500
Emission, nm	280 – 330	300 – 350	380 – 600	280 – 380	380 – 600

For qualitative analysis, spectra are represented in A.U. (Arbitrary Unit) and rejected fraction spectra (R) were calculated by subtracting permeate spectra from the BSN spectra, in order to better visualize the constituents that are rejected by the membrane. For semi-quantitative analysis, the volume of fluorescence Φ(i) (Raman Unit.nm^2) normalized by the Raman spectra,[66] consisting of the integration of the spectral regions, was calculated in the different spectral regions using the following equation taken from the fluorescence regional integration (FRI)[54] method:

$$\Phi(i) = MF(i) \sum_{ex} \sum_{em} I(\lambda_{ex}\lambda_{em}) \Delta\lambda_{ex} \Delta\lambda_{em} \quad \text{(Eq. 1)}$$

where MF(i) is a multiplication factor, $\Delta\lambda_{ex}$ is the excitation wavelength interval (2 nm), $\Delta\lambda_{em}$ is the emission wavelength interval (0.5 nm) and $I(\lambda_{ex}\lambda_{em})$ is the fluorescence intensity at each excitation-emission pair (Raman units). $\Phi(i)$ normalization was necessary to compare values from different regions of the 3DEEM response. To do so, $MF(i)$ was calculated using Equation 2.

$$MF(i) = \frac{Total\ spectra\ area}{Specific\ region\ area(i)} \quad \text{(Eq. 2)}$$

For percentage analysis, the ratio between the volume of fluorescence of each region and the total volume was used.

2.5. Photochemical experiments

Photochemical experiments were conducted in an enclosed UV cabinet with a magnetically stirred photoreactor at room temperature. A 15 W low pressure mercury lamp (Sankyo Denki Co.,) was used as a UVC light source. The distance between the light source and reaction vessel was 20 cm. The irradiance at 254 nm at the location of the vessel was measured to be 295 μW/cm^2 with a BLUE-Wave UVNb-25 Spectrometer (StellarNet Inc., Tampa, FL). The UV/Vis emission spectrum for the lamp, shown in Figure S1, was also recorded. The DOM fractions and EfOM samples described above,

along with HA, were used to show the inhibitory effect of organic matter on photocatalytic degradation of target pollutants. Experiments utilized 15 ml of solution, containing 5 µg/L TiO_2 with 10 µM para-chlorobenzoic acid (*p*CBA) as a probe compound that has a known reaction rate constant with ·OH.[30] HA, DOM fractions, or EfOM samples in various concentrations were added to the reaction solutions to assess the quenching potential of each fraction. Sample aliquots of 0.5 mL were taken at fixed time points and analyzed for *p*CBA concentration via HPLC, according to methods reported elsewhere.[67] Briefly, this analysis was conducted with an Agilent HPLC (Agilent technology, 1260 infinity) using a C18 (125 mm) column using acetonitrile and 10 mM phosphoric acid as mobile phase solvents (60:40). The flow rate was 0.5 mL/min and the detection wavelength was 234 nm. For all photochemical reactions, *p*CBA degradation rates were obtained by linear regression of plots of *p*CBA concentration versus radiant fluence (µJ/cm^2). Fluence values were calculated according to Bolton and Linden (2003),[68] as described previously.[57] Importantly, these calculations account for reductions in UV_{254} transmission by using sample-specific UV_{254} absorbance values and the transmission distance inside the reactor. The resulting observed photodegradation rates (k_{obs}) were, to a good approximation, first order with respect to radiant exposure (H, µJ/cm^2) such that the units of k_{obs} are reported as (cm^2/µJ), according to equations (3-6):

$$\frac{dC}{dt} = k'_{obs}C, \quad \text{(Eq. 3)}$$

$$\frac{1}{H(\mu J/cm^2)}\frac{dC}{dt} = \frac{1}{H(\mu J/cm^2)}k'_{obs}C, \quad \text{(Eq. 4)}$$

$$\frac{dC}{dH} = k_{obs}C, \quad \text{(Eq. 5)}$$

and

$$k_{obs}\left(\frac{cm^2}{\mu J}\right) = \frac{k'_{obs}(\frac{1}{s})}{E(\frac{\mu W}{cm^2})}. \quad \text{(Eq. 6)}$$

Here, k'_{obs} (s^{-1}) is the first-order degradation rate constant of *p*CBA, C is the molar concentration of *p*CBA, and E is the irradiance (µW/cm^2) at 254 nm. The differences in the k_{obs} in the presence or absence of organic compounds were used to quantify the inhibitory effect of these compounds. Control experiments were also conducted in the absence of organic matter, TiO_2, or light.

3. Results

3.1. Isolated DOM fractions

Prior to performing photocatalytic experiments, DOM fractions were characterized using 3DEEM to identify molecular characteristics of DOM within each fraction. The 3DEEM spectra compiled for the fractions are available elsewhere[23] and were used here to quantify the volume of fluorescence and the percentage of fluorescence of each region in Figure 1.

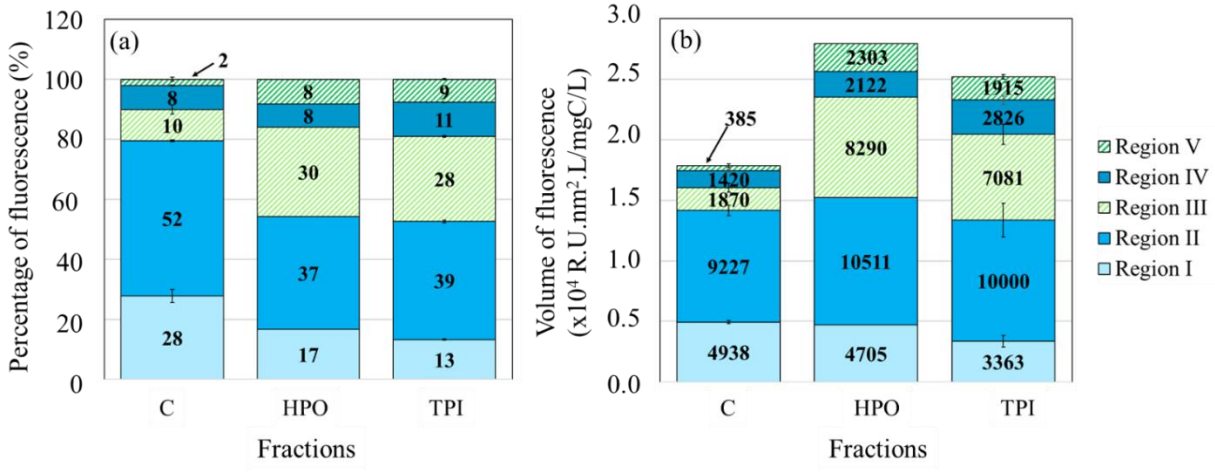

Figure 1. (a) Percentage of fluorescence and (b) Volume of fluorescence of the colloidal (C), HPO and TPI fractions prepared at 1 mgC/L. Region I, Region II, Region III, Region IV and Region V correspond to aromatic proteins-like type I, aromatic proteins-like type II, fulvic-like, SMP-like and humic-like fluorophores, respectively.

3DEEM analysis showed that each of the three DOM fractions contained both classes of fluorescent compounds: proteins (Regions I, II and IV) and humic substances (Region III and V). However, as seen in Figure 1a, DOM fractions exhibited different fluorescent properties, reflecting differences in their compositions. The percentages of fluorescence of HPO and TPI fractions were similar for all regions and had a dominant proportion of aromatic protein-like type II and fulvic-like fluorophores (Figure 1a). That HPO and TPI compositions did not vary significantly in terms of fluorophore content expected; a study on EfOM of wastewater treatment plants also found that these fractions were similar in terms of fluorophore composition.[69] For the colloidal fraction, 80% of the fluorescent compounds were aromatic protein-like type I and II fluorophores. Recent studies showed that both protein-like and humic-like fluorophores impact photocatalytic performance. Protein-like constituents were found to

282 react with ·OH radicals in bulk solution,[55] with reported reaction rate constants of amino acids,
283 proteins, and peptides with ·OH ranging from 1.7×10^{7} to 1.05×10^{10} M^{-1} s^{-1} (the rate constant between
284 *p*CBA and ·OH is similar at 5.2×10^{9} M^{-1} s^{-1}),[70-72] while humic-like compounds, having a large number
285 of carboxylic groups, adsorbed onto TiO_2 surfaces, particularly at low pHs.[73] Thus, the high proportion
286 of fluorescing compounds in Region I and II in colloids, suggests that the colloids may be more
287 reactive with ·OH than HPO and TPI. On the contrary, HPO and TPI are expected to exhibit more
288 surface-phase quenching by adsorbing more strongly onto TiO_2 and than the colloids.

289 The volume of fluorescence is an indicator proportional to the concentration of fluorophores contained
290 in each region. The higher electron density of fluorophores compared with other moieties could yield
291 higher reactivity with ROS, and it would follow, then, that the higher the volume of fluorescence, the
292 higher the quenching of photocatalysis. Thus, from Figure 2b, and hypothesizing that surface-phase
293 quenching is the most problematic for photocatalysis, the DOM quenching potency could be expected
294 in the following order: HPO>TPI>C. A similar analysis can be conducted by measuring the $SUVA_{254}$
295 values as a representation of average aromatic moiety content, which is known to loosely indicate
296 DOM hydrophilicity.[74] In general, DOM compounds with higher $SUVA_{254}$ values are considered to be
297 more hydrophobic than those with lower values.[75] In addition, higher $SUVA_{254}$ values correspond to
298 more aromaticity, which could indicate higher reactivity with ROS, given the electron rich moieties.
299 The $SUVA_{254}$ values for the colloidal, HPO, and TPI fractions were measured to be 1.8, 2.2, and 1.6
300 $L.mg^{-1}.m^{-1}$, respectively. Based on this method of analysis, and assuming that electron-dense
301 functional groups are the primary factor in determining ROS quenching, the inhibition capacity of the
302 fractions could be expected in this order: HPO>C>TPI. Neither of these methods are expected to
303 conclusively predict the true inhibition potential, given the many additional factors involved with
304 quenching mechanisms.

305 3.2. EfOM composition and effect of membrane fouling

306 To estimate the effect of membrane fouling and cleaning on the retention of fluorophores, 3DEEM
307 spectra of MBR bulk supernatant and permeate were compared (Figure 2). The membranes rejected
308 most compounds from Regions I and II in the three MBR cases studied. This selectivity was apparent

in the 3DEEM spectra obtained by subtracting the permeate spectrum from the BSN spectrum. It is likely that most of these aromatic-like fluorophores were associated with organic colloids since they represented 80% of the overall colloidal content. This observation is consistent with a previous study that demonstrated that colloids were major membrane foulants.[23]

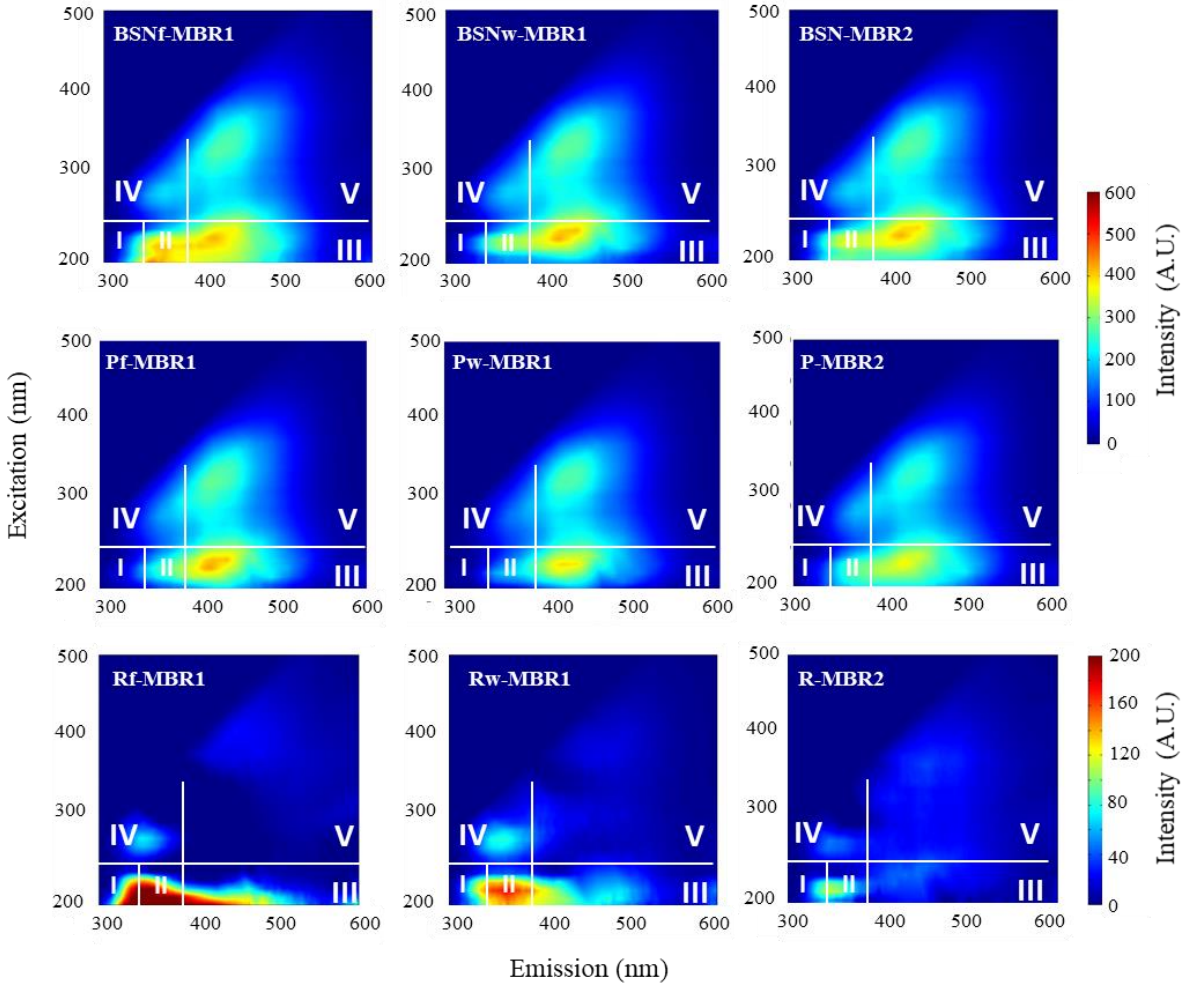

Figure 2. Fluorescence spectra of DOM from BSN and EfOM from permeate samples, with I, II, III, IV, V corresponding to Region I (aromatic proteins-like type I), Region II (aromatic proteins-like type II), Region III (fulvic-like), Region IV (SMP-like) and Region V (humic-like). R spectra correspond to the mathematical subtraction of the permeate spectra from the bulk supernatant spectra allowing the identification of compounds retained by the membrane. Note the different color scale for the R spectra.

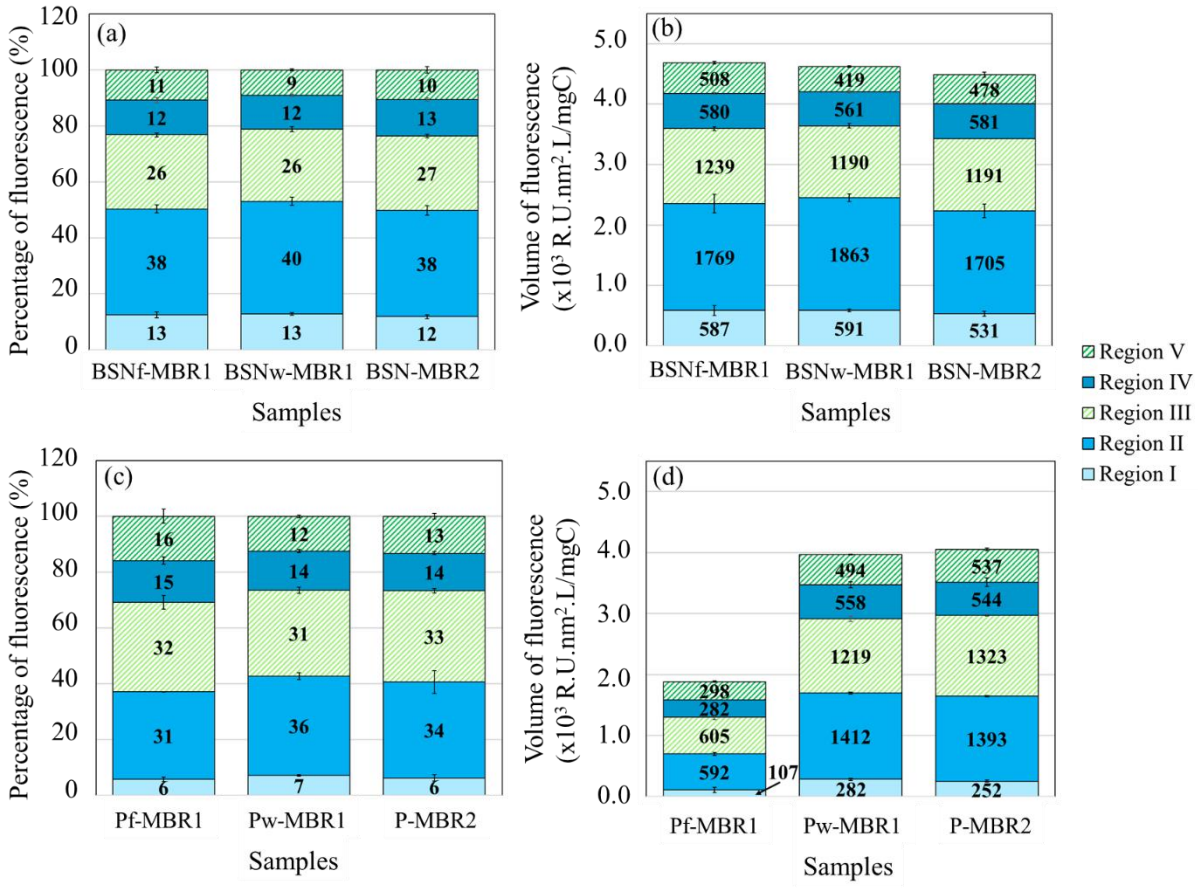

Figure 3. Percentage (a, c) and volume (b, d) fluorescence values for bulk supernatant (a, b) and permeate (c, d) samples.

Figures 3a and 3c show the fluorophore compositions in EfOM samples as percentages of the different regions; these data showed a preferential rejection of the fluorophores from Region I and Region II. Indeed, for the three samples, the membrane reduced the fluorescence by 11 ± 2 % in both Region I and II. This reduction corresponded to an increase of fluorescence percentage of the Regions III and V in the permeate. The relative increase of the humic substance-related fluorophores confirmed that the membrane preferentially retains colloids, since they are typically high molecular weight molecules associated with protein-like fluorophores (Figure 1a).[53] Membrane fouling clearly affected the type of fluorophores retained in the MBR (Figure 3b and Figure 3d). The three fouling stages present similar bulk supernatant volumes of fluorescence (Figure 3b) and permeate percentage of fluorescence profiles (Figure 3c), but different volumes of fluorescence in the permeate (Figure 3d). The TOC normalized volume of fluorescence for Pf-MBR1 was reduced by 60% (Figure 3b and Figure 3d),

while the volume of fluorescence was only reduced by 14% and 10% for P-MBR2 and Pw-MBR1, respectively (Figure 3b and Figure 3d). Membrane fouling therefore has a clear effect on fluorophore quantity, via restricting EfOM permeation (Figure 3b). Indeed, more fluorescent compounds are retained, on a per carbon basis, by a fouled membrane. This result shows that the fouling layer on the membrane surface selectively removes compounds rich in functional groups with high electron density, which are more reactive with ROS than other moieties. Pw-MBR1 and P-MBR2 are therefore expected to quench photocatalysis to a greater extent. This assumption is supported by the $SUVA_{254}$ data: values for the Pf-MBR1, Pw-MBR1, and P-MBR2 samples were measured to be 0.8, 2.0, and 2.0 $L \cdot mg^{-1} \cdot m^{-1}$, respectively. Pf-MBR1, having a $SUVA_{254}$ value of 0.8 $L \cdot mg^{-1} \cdot m^{-1}$, is characterized by non-aromatic organic compounds and therefore fewer potential functional groups reactive with ROS. On the contrary, Pw-MBR1 and P-MBR2, with $SUVA_{254}$ values of 2.0 $L \cdot mg^{-1} \cdot m^{-1}$, contain more aromatic compounds, which may preferentially compete with ROS.

Control of membrane fouling may provide an opportunity to increase photocatalysis process efficiency by regulating the chemical makeup and concentration of EfOM. Less frequent cleaning events could be ideal, since the fouled membranes provided the highest DOM retention. From the fluorescence volumes, it is expected that TiO_2 photocatalysis would be quenched to a greater extent by Pw-MBR1 and P-MBR2, than by Pf-MBR1.

3.3. Inhibition of ·OH by DOM Fractions

Segregation of MBR DOM into functional categories allowed for a unique examination of the inhibition potential of these functional classes of compounds. Colloidal, HPO, and TPI fractions were each examined for concentration-dependent inhibitory activity. Control tests confirmed the photocatalytic action of TiO_2 and differentiated the role of ROS from the direct photolysis by UV_{254} light (Figure S3). The action by UV_{254} alone represented the lower bound of $k_{obs,pCBA}$, where ·OH radicals were completely quenched by DOM. Likewise, the case of TiO_2 and *p*CBA in pure water served as the upper bound of photocatalytic efficiency, with no interfering quenching agents. The $k_{obs,pCBA}$ values plotted in Figure 4 showed that of the three DOM fractions, colloids exerted the strongest inhibition by far. The corresponding k'_{obs} (s^{-1}) data is shown in Figure S4. The TPI and HPO

366 portions were similar in their effect on $k_{obs,pCBA}$, and exerted mild inhibition at low TOC
367 concentrations. Interestingly, for both TPI and HPO, the $k_{obs,pCBA}$ increased from 7.5 to 10 mgC/L. This
368 increase in photodegradation efficacy was surprising but not unprecedented; it was recently reported
369 that Natural Organic Matter (NOM) actually enhanced the TiO_2-driven photodegradation of
370 carbamazepine, pharmaceutical compound, at specific TiO_2:NOM ratios, by up to 8%.[76] Favorable
371 NOM-carbamazepine interactions explained the increased effectiveness; these interactions draw the
372 compound closer to the active surface sites of TiO_2, where ·OH are present at higher concentrations.
373 The colloidal fraction did not increase the photoactivity at any concentration. Examination of the
374 inhibition profiles of the three DOM fractions in the context of 3DEEM analysis (Figure 1) suggested
375 that the quenching action of the DOM fractions is correlated to higher concentration of colloids, which
376 are characterized by a higher proportion of fluorescence in Region I and Region II (Figure 1a). This
377 observation suggests that despite higher volumes of fluorescence, HPO and TPI are less potent
378 inhibitors of photocatalysis than the colloids. The surface interactions, and therefore inhibition
379 mechanism, of the colloids with the TiO_2 surface could be fundamentally different from that of the
380 HPO and TPI fractions, because the colloidal fraction was not segregated based on surface character,
381 but rather by size only. Control of membrane surface properties and fouling could reduce the colloidal
382 content—much of which consists of high molecular weight molecules that can be preferentially
383 retained—in EfOM and thereby mitigate the quenching of photocatalytic processes by DOM.[23]

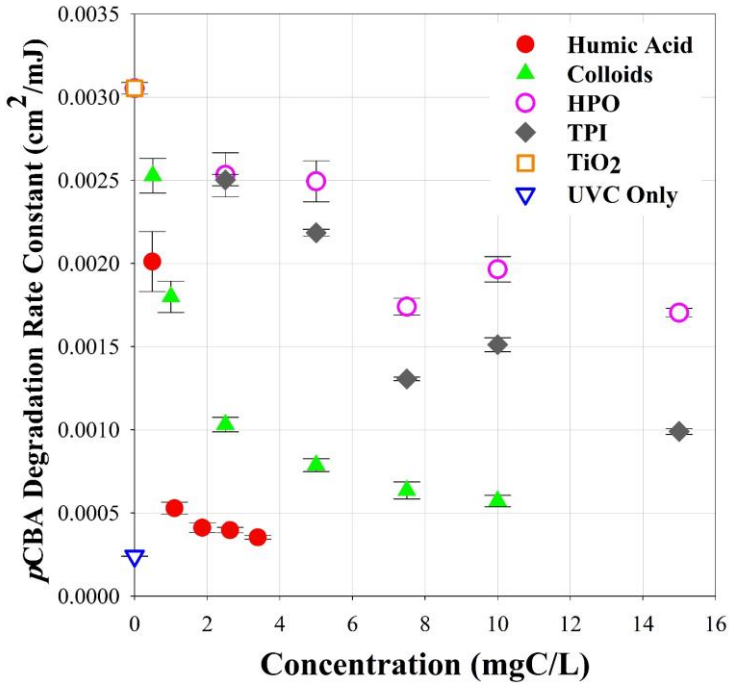

Figure 4: *p*CBA degradation rate constants in the presence of 5 mg/L TiO_2 and various concentrations of colloids, TPI, HPO, and HA are depicted here. The rate constant for *p*CBA degradation by UVC without TiO_2 is also shown. Ambient temperature was measured at 24 °C.

3.4. Inhibition of ·OH by EfOM

The EfOM of the three MBR permeate samples, as described above, was tested for inhibition potential of ·OH-mediated *p*CBA degradation. The samples were examined on a TOC basis to discern changes in inhibition potential caused by qualitative differences in EfOM composition. A low concentration of TiO_2, relative to that used in similar studies on photocatalyst-DOM interactions,[29, 38, 77, 78] was selected to avoid the effects of EfOM transformation by oxidation. Hour-long UVC irradiation experiments with 10 mg/L HA and various concentrations of TiO_2 showed that *p*CBA photodegradation kinetics were linear for the TiO_2 concentration of 5 mg/L. Tests with TiO_2 concentrations of 100 mg/L or higher showed accelerating kinetics and suggested that HA was itself being degraded by ·OH radicals so that its inhibition potential changed with time.

The inhibition capacities of MBR EfOM samples were evaluated by measuring $k_{obs,pCBA}$ as a function of individual EfOM sample concentrations. These rates were calculated across concentrations ranging

401 from 0 to 2.3 mgC/L (Figure 5). The corresponding k'$_{obs}$ (1) data is shown in Figure S5. Comparing
402 $k_{obs,pCBA}$ values for the same TOC content reveals that the state of membrane fouling drove clear
403 distinctions in inhibitory activity of the EfOM. While it was expected that a fouled membrane would
404 reject more DOM than a clean membrane, the inhibition capacity on a per carbon basis was not
405 known. Here, it was observed that EfOM from a fouled membrane system inhibited the photocatalytic
406 process much less than EfOM from a cleaned membrane. At just 0.5 mgC/L, Pw-MBR1 quenched the
407 photocatalytic process completely, while no quenching was observed by Pf-MBR1 EfOM at the same
408 concentration. This result provides evidence that the changes in EfOM composition caused by
409 membrane fouling; the reduction of colloid concentration and total fluorophores is especially
410 beneficial for photocatalytic operation. 3DEEM confirmed that molecules containing fluorescent
411 groups in Regions I and II impact photocatalytic performance more than other compounds. Qualitative
412 changes in DOM retention by the membrane, therefore, impacted the photocatalytic quenching
413 process. Considering these results in the context of the DOM fractions analysis, retention of organic
414 colloids by the fouled membrane was likely enhanced by the formation of a fouling layer.[3, 22]
415 Inhibition by P-MBR2, sourced from a membrane at the midpoint between chemical cleanings, was
416 between the two extremes of Pw- and Pf-MBR1, with a ~75% reduction in $k_{obs,pCBA}$ at 0.5 mgC/L.
417 Alternatively, it may be possible to choose or modify membrane materials to selectively reject the
418 organic colloidal materials regardless of the fouling state. HA served as a reference material, which
419 represents NOM found in drinking water sources more closely than EfOM, and exhibited stronger
420 quenching than the P-MBR2 case but less inhibition than Pw-MBR1. It is noteworthy that HA inhibits
421 TiO_2 driven photocatalysis to a greater extent than EfOM from a fouled MBR on a carbon basis. This
422 finding contradicts a 'common sense' assumption that could be made based solely on TOC values: that
423 photocatalysis would be more applicable for drinking water applications than for WWTP effluent.

424 The 3DEEM analyses (Figure 3) of the MBR EfOM samples predicted that the fouled membrane
425 would reduce the quantity of fluorescent compounds in the EfOM and therefore lead to less inhibition
426 of photocatalysis. However, for cases of similar fluorescence volumes, as for Pw-MBR1 and P-MBR2
427 in particular, the use of 3DEEM did not explain differences in inhibitory action. In these cases, other

factors, such as the hydrophobic/hydrophilic character of the EfOM, may have been altered by the membrane fouling but not detected by 3DEEM or TOC analysis. It is well known that membrane fouling affects rejection of DOM components[41, 43, 79] and that the mechanism of action is not simply size exclusion alone: changes in the surface characteristics (i.e. charge and hydrophobicity), due to fouling layer formation, are also important.[3, 22]

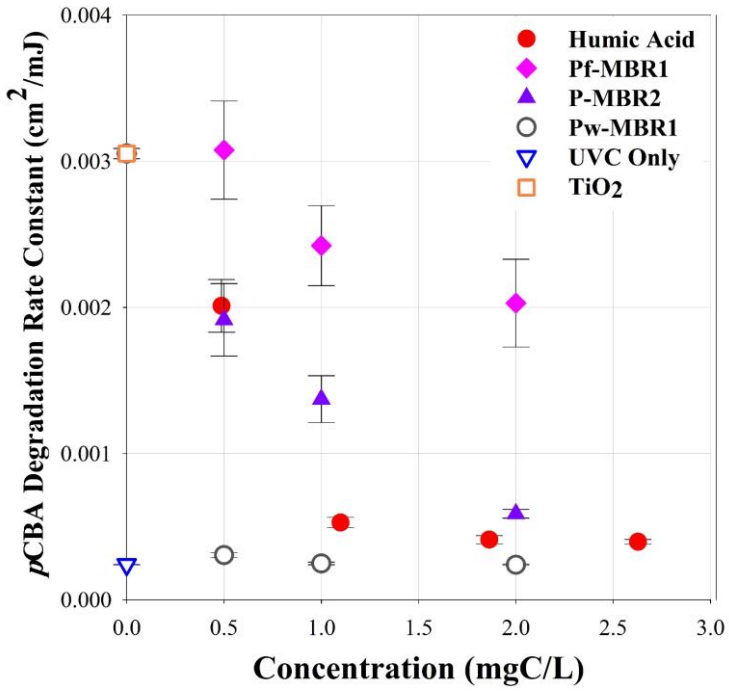

Figure 5: *p*CBA degradation rate constants in the presence of various concentrations of HA, effluents from Pf-MBR1, from Pw-MBR1, and from P-MBR2 with 5 mg/L TiO_2 are depicted here. The rate constant for pCBA degradation by UVC without TiO_2 is also shown.

3.5. Inhibitory mechanisms for DOM samples

Identification of the mechanism of inhibition by DOM on TiO_2 photocatalysis is the key to designing processes to overcome the problem of ROS quenching. Numerous studies have evaluated the adsorption interactions of NOM onto TiO_2, fitting experimental findings to Freundlich[80] or Langmuir-Hinshelwood[32, 77, 81] isotherms. Only recently, however, was a model developed that accounted for both bulk- and surface-phase quenching interactions.[29] In their work, Brame et al. experimentally validated a model that combined a multi-solute Langmuir model[82] with bulk phase competitive

445 reaction rates by assuming steady-state ROS concentrations.[29] Based on this dual-phase model, the
446 mode of inhibition (bulk or surface reactions) was successfully predicted by analysis of the
447 dependency of k_{obs} on TOC. A linear dependence of $k_{obs,}$ on TOC implied that inhibition primarily
448 occurred in the bulk phase and surface interactions were unimportant; alternatively, an exponential
449 decay of k_{obs} with increasing TOC indicated that surface sorption and reactions played a significant
450 role in the inhibitory process.[29] Note that the aforementioned report used Suwannee River humic acid
451 as an NOM source, which consists of a wide range of molecules;[29] applying Brame's model in
452 experiments with fractionated DOM samples is an important extension of the earlier work allowing for
453 a discriminating analysis of inhibition mechanisms across the DOM spectrum. Here, all experiments
454 were performed with the same probe compound, photocatalyst concentration, and UV_{254} lamp, so
455 normalization of $k_{obs,pCBA}$ was not necessary. The inhibition profile for HA was non-linear and
456 therefore depended on surface interactions, in line with previous reports for TiO_2 inhibition by
457 NOM.[29, 38, 83, 84] Upon examination of the inhibitory profiles of the MBR effluents, trends for Pf-MBR1
458 and P-MBR2 were noted to be nearly linear, whereas Pw-MBR1 showed an exponential relationship.
459 These observations suggest that the membrane fouling layer played a critical role by rejecting DOM
460 that adsorbs favorably onto the surface of TiO_2, thereby exerting a strong quenching effect on
461 photocatalytic processes. These observations correlate well with the observed inhibition profiles of the
462 fractionated DOM.

463 As discussed, the colloidal fraction of BSN DOM exerted the strongest inhibitory action of any of the
464 fractions (Figure 4). The $k_{obs,pCBA}$ inhibition profiles of the DOM fractions reveal that the colloids
465 quenched the photocatalytic process via sorption onto the TiO_2 surface and reacting with surface-
466 bound ·OH. The HPO and TPI fractions, however, displayed a linear dependence—if the spurious
467 enhancement of $k_{obs,pCBA}$ at the 10 mgC/L mark is neglected—on TOC. The HPO and TPI samples,
468 therefore, primarily reduced $k_{obs,pCBA}$ through bulk phase reactions limited by diffusion and relative
469 reaction rates. Note that these remarks on quenching mechanisms are generalizations: even the
470 fractionated DOM samples contain a wide variety of molecules, each with specific adsorption
471 affinities and reaction rates. Still, results of both fractionation and membrane fouling conditions

showed significant changes to inhibitory action of DOM. The inhibitory action of the colloidal fraction was particularly interesting, given the lack of inhibitory action by effluent from the fouled membrane. These observations taken together in Figure 6 (data replotted from Figures 4 and 5) suggest that fouled membranes reject key organic colloids that would otherwise adsorb strongly to TiO_2 surfaces and greatly reduce photodegradation rates. The corresponding k'_{obs} (s^{-1}) data is shown in Figure S6. The prospective utility of a membrane for pretreatment is clearly demonstrated by these results: if a membrane can be selected or optimized to reject problematic colloids, photocatalysis may indeed be effective for disinfection of MBR effluent.

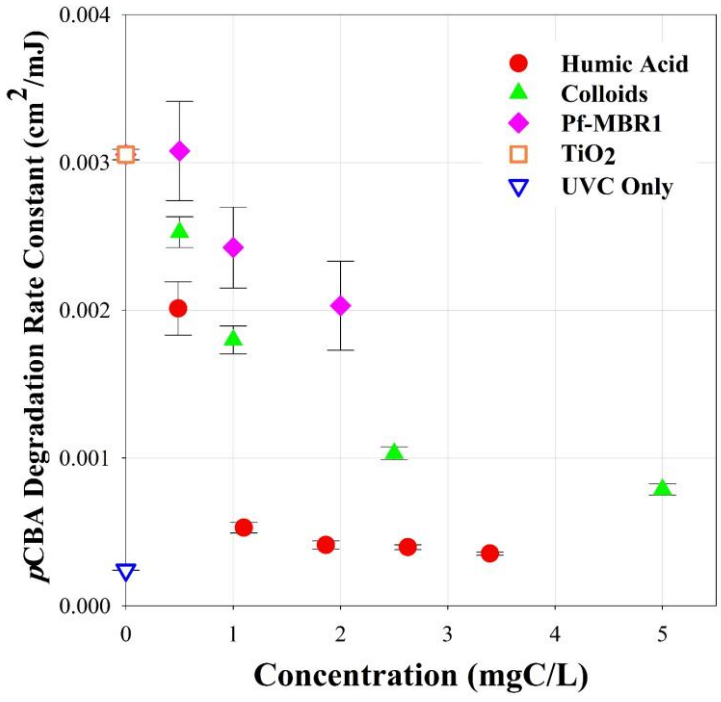

Figure 6: $k_{obs,pCBA}$ inhibition profiles of HA, Pf-MBR1, and the colloidal fraction. Data from Figures 3 and 4 are used here.

4. Conclusions

The challenge of unwanted ROS-DOM reactions has long plagued photocatalysis, particularly for applications dealing with high TOC concentrations such as in a typical MBR effluent. 3DEEM can be

used to predict the inhibitory effects of DOM composition, and the experiments shed new light on the quenching of photocatalysts by DOM. First, the total fluorescence volume correlated well with the extent of photocatalytic inhibition on a carbon basis, further the DOM fractionation demonstrated that the colloidal fraction of DOM exerted stronger quenching action than HPO and TPI. The membrane fouling status showed that fouled membrane showed very little inhibitory action compared to permeate from clean and moderately fouled membranes. In fact, DOM from fouled membrane appeared to quench ·OH primarily via bulk-phase scavenging, whereas DOM from a clean membrane showed an inhibition profile consistent with surface-phase reactions,[28] suggesting that the membrane fouling layer rejected materials that would otherwise adsorb strongly to the TiO2 surface. To enhance photocatalysis efficiency, it might be possible to select a membrane with a "built-in" selectivity similar to that of the fouled membrane in order to remove the problematic colloidal fraction. Analysis of the inhibition profiles of the EfOM described here suggests that for the operation of a PMR a trade-off can be made between the operational pressure and the photocatalytic efficiency; by reducing the (chemical) cleaning frequency and thereby maintaining a minimal level of fouling, inhibition of photocatalysis by organic colloidal inhibitors would be mitigated at a cost of higher trans-membrane pressures. Further, the surface coverage of TiO_2 on PMRs can be tuned to optimize photocatalyst surface area[85] and may not be limited to the DOM:TiO_2 ratios explored here.

Further research on the fundamental surface interactions between these organic colloidal materials and photocatalyst or membrane surfaces should be pursued in order to develop mitigation strategies for DOM-related ROS inhibition. Specifically, the assessment of the potential effects of the hydrophilic fraction and dissolved ions (i.e., multivalent cations and halides), which were not retained by the fractionation processes, should be examined. The results of the present study may be applicable to the use of photocatalytic materials in systems containing other DOM sources, therefore additional investigations on systems such as potable water supplies or industrial waste streams would be timely and important.

5. Acknowledgements

This material is based upon work supported in part by the Louisiana Board of Regents Research Competitiveness Subprogram under grant LEQSF(2017-20)-RD-A-06 and in part by the National Science Foundation Partnerships for International Research and Education program under Grant IIA-1243433. The authors would like to thank the operators at the La Grande Motte wastewater treatment plant for providing access to their facility and assistance with collecting wastewater samples for analysis.

6. References

1. R. L. Droste, *Theory and Practice of Water and Wastewater Treatment*, John Wiley & Sons, Inc., New York, 1997.
2. L. B. Franklin, *Wastewater Engineering: Treatment, Disposal and Reuse*, McGraw Hill, Inc., New York, 1991.
3. O. T. Iorhemen, R. A. Hamza and J. H. Tay, Membrane Bioreactor (MBR) Technology for Wastewater Treatment and Reclamation: Membrane Fouling, *Membranes*, 2016, **6**, 1-29.
4. D. S. Francy, E. A. Stelzer, R. N. Bushon, A. M. G. Brady, A. G. Williston, K. R. Riddell, M. A. Borchardt, S. K. Spencer and T. M. Gellner, Comparative effectiveness of membrane bioreactors, conventional secondary treatment, and chlorine and UV disinfection to remove microorganisms from municipal wastewaters, *Water Res.*, 2012, **46**, 4164-4178.
5. E. O'Brien, M. Munir, T. Marsh, M. Heran, G. Lesage, V. V. Tarabara and I. Xagoraraki, Diversity of DNA viruses in effluents of membrane bioreactors in Traverse City, MI (USA) and La Grande Motte (France), *Water Res.*, 2017, **111**, 338-345.
6. Y. P. Zhang and J. L. Zhou, Occurrence and removal of endocrine disrupting chemicals in wastewater, *Chemosphere*, 2008, **73**, 848-853.
7. Y. L. Luo, W. S. Guo, H. H. Ngo, L. D. Nghiem, F. I. Hai, J. Zhang, S. Liang and X. C. C. Wang, A review on the occurrence of micropollutants in the aquatic environment and their fate and removal during wastewater treatment, *Sci. Total Environ.*, 2014, **473**, 619-641.
8. M. Munir, K. Wong and I. Xagoraraki, Release of antibiotic resistant bacteria and genes in the effluent and biosolids of five wastewater utilities in Michigan, *Water Res.*, 2011, **45**, 681-693.
9. I. Kim, N. Yamashita and H. Tanaka, Performance of UV and UV/H2O2 processes for the removal of pharmaceuticals detected in secondary effluent of a sewage treatment plant in Japan, *J. Hazard. Mater.*, 2009, **166**, 1134-1140.
10. M. Klavarioti, D. Mantzavinos and D. Kassinos, Removal of residual pharmaceuticals from aqueous systems by advanced oxidation processes, *Environ. Int.*, 2009, **35**, 402-417.
11. L. Yang, L. E. Yu and M. B. Ray, Degradation of paracetamol in aqueous solutions by TiO2 photocatalysis, *Water Res.*, 2008, **42**, 3480-3488.
12. Y. J. Meng, Y. Wang, Q. Han, N. Xue, Y. Y. Sun, B. Y. Gao and Q. L. Li, Trihalomethane (THM) formation from synergic disinfection of biologically treated municipal wastewater: Effect of ultraviolet (UV) irradiation and titanium dioxide photocatalysis on dissolve organic matter fractions, *Chem. Eng. J.*, 2016, **303**, 252-260.
13. J. C. Crittenden, R. Rhodes Trussell and D. W. Hand, *MWH's Water Treatment: Principles and Design*, John Wiley & Sons, Inc. , Hoboken, New Jersey, 2012.
14. W. A. M. Hijnen, E. F. Beerendonk and G. J. Medema, Inactivation credit of UV radiation for viruses, bacteria and protozoan (oo)cysts in water: A review, *Water Res.*, 2006, **40**, 3-22.

15. M. Cho, H. M. Chung, W. Y. Choi and J. Y. Yoon, Different inactivation Behaviors of MS-2 phage and Escherichia coli in TiO2 photocatalytic disinfection, *Appl. Environ. Microbiol.*, 2005, **71**, 270-275.
16. S. D. Snow, K. Park and J.-H. Kim, Cationic Fullerene Aggregates with Unprecedented Virus Photoinactivation Efficiencies in Water, *Environ. Sci. Tech. Let.*, 2014, **1**, 290-294.
17. S. Malato, P. Fernandez-Ibanez, M. I. Maldonado, J. Blanco and W. Gernjak, Decontamination and disinfection of water by solar photocatalysis: Recent overview and trends, *Catal. Today*, 2009, **147**, 1-59.
18. M. Cho, H. Chung, W. Choi and J. Yoon, Linear correlation between inactivation of E. coli and OH radical concentration in TiO2 photocatalytic disinfection, *Water Res*, 2004, **38**, 1069-1077.
19. J. A. Grant and R. Hofmann, A comparative study of the hydroxyl radical scavenging capacity of activated sludge and membrane bioreactor wastewater effluents, *Water Sci. Technol.*, 2016, **73**, 2067-2073.
20. S. Tang, Z. Wang, Z. Wu and Q. Zhou, Role of dissolved organic matters (DOM) in membrane fouling of membrane bioreactors for municipal wastewater treatment, *J. Hazard. Mater.*, 2010, **178**, 377-384.
21. K. Chon, K. Lee, I.-S. Kim and A. Jang, Performance assessment of a submerged membrane bioreactor using a novel microbial consortium, *Bioresour. Technol.*, 2016, **210**, 2-10.
22. C. Jarusutthirak, G. Amy and J.-P. Croué, Fouling characteristics of wastewater effluent organic matter (EfOM) isolates on NF and UF membranes, *Desalination*, 2002, **145**, 247-255.
23. C. Jacquin, B. Teychene, L. Lemee, G. Lesage and M. Heran, Characteristics and fouling behaviors of Dissolved Organic Matter fractions in a full-scale submerged membrane bioreactor for municipal wastewater treatment, *Biochem. Eng. J.*, 2018, **132**, 169-181.
24. P. Wang, Z. W. Wang, Z. C. Wu and S. H. Mai, Fouling behaviours of two membranes in a submerged membrane bioreactor for municipal wastewater treatment, *J. Membr. Sci.*, 2011, **382**, 60-69.
25. C. Kunacheva, C. Le, Y. N. A. Soh and D. C. Stuckey, Chemical Characterization of Low Molecular Weight Soluble Microbial Products in an Anaerobic Membrane Bioreactor, *Environ. Sci. Technol.*, 2017, **51**, 2254-2261.
26. J. Y. Sun, K. Xiao, Y. H. Mo, P. Liang, Y. X. Shen, N. W. Zhu and X. Huang, Seasonal characteristics of supernatant organics and its effect on membrane fouling in a full-scale membrane bioreactor, *J. Membr. Sci.*, 2014, **453**, 168-174.
27. K. Xiao, Y. X. Shen, S. Liang, P. Liang, X. M. Wang and X. Huang, A systematic analysis of fouling evolution and irreversibility behaviors of MBR supernatant hydrophilic/hydrophobic fractions during microfiltration, *J. Membr. Sci.*, 2014, **467**, 206-216.
28. S. Giannakis, S. Liu, A. Carratalà, S. Rtimi, M. Talebi Amiri, M. Bensimon and C. Pulgarin, Iron oxide-mediated semiconductor photocatalysis vs. heterogeneous photo-Fenton treatment of viruses in wastewater. Impact of the oxide particle size, *J. Hazard. Mater.*, 2017, **339**, 223-231.
29. J. Brame, M. Long, Q. Li and P. Alvarez, Inhibitory effect of natural organic matter or other background constituents on photocatalytic advanced oxidation processes: Mechanistic model development and validation, *Water Res*, 2015, **84**, 362-371.
30. G. V. Buxton, C. L. Greenstock, W. P. Helman and A. B. Ross, Critical review of rate constants for reactions of hydrated electrons, hydrogen atoms and hydroxyl radicals (.OH/.O-) in aqueous solution, *J. Phys. Chem. Ref. Data*, 1988, **17**, 513-886.
31. S. Kim and W. Choi, Kinetics and mechanisms of photocatalytic degradation of (CH3)(n)NH4-n+ (0 <= n <= 4) in TiO2 suspension: The role of OH radicals, *Environ. Sci. Technol.*, 2002, **36**, 2019-2025.
32. R. Enriquez and P. Pichat, Interactions of Humic Acid, Quinoline, and TiO2 in Water in Relation to Quinoline Photocatalytic Removal, *Langmuir*, 2001, **17**, 6132-6137.
33. C. Kunacheva, Y. N. A. Soh, A. P. Trzcinski and D. C. Stuckey, Soluble microbial products (SMPs) in the effluent from a submerged anaerobic membrane bioreactor (SAMBR) under different HRTs and transient loading conditions, *Chem. Eng. J.*, 2017, **311**, 72-81.

34. Y. Yang, J. J. Pignatello, J. Ma and W. A. Mitch, Effect of matrix components on UV/H2O2 and UV/S2O82− advanced oxidation processes for trace organic degradation in reverse osmosis brines from municipal wastewater reuse facilities, *Water Res.*, 2016, **89**, 192-200.
35. F. L. Rosario-Ortiz, E. C. Wert and S. A. Snyder, Evaluation of UV/H2O2 treatment for the oxidation of pharmaceuticals in wastewater, *Water Res.*, 2010, **44**, 1440-1448.
36. N. Senesi, Binding mechanisms of pesticides to soil humic substances, *Sci. Total Environ.*, 1992, **123-124**, 63-76.
37. J. D. Ritchie and E. M. Perdue, Proton-binding study of standard and reference fulvic acids, humic acids, and natural organic matter, *Geochim. Cosmochim. Acta*, 2003, **67**, 85-96.
38. J. Brame, M. C. Long, Q. L. Li and P. Alvarez, Trading oxidation power for efficiency: Differential inhibition of photo-generated hydroxyl radicals versus singlet oxygen, *Water Res.*, 2014, **60**, 259-266.
39. P. R. Ogilby, Singlet oxygen: there is indeed something new under the sun, *Chem. Soc. Rev.*, 2010, **39**, 3181-3209.
40. Z. X. Cai and M. M. Benjamin, NOM Fractionation and Fouling of Low-Pressure Membranes in Microgranular Adsorptive Filtration, *Environ. Sci. Technol.*, 2011, **45**, 8935-8940.
41. L. Fan, J. L. Harris, F. A. Roddick and N. A. Booker, Influence of the characteristics of natural organic matter on the fouling of microfiltration membranes, *Water Res.*, 2001, **35**, 4455-4463.
42. E. Filloux, H. Gallard and J.-P. Croue, Identification of effluent organic matter fractions responsible for low-pressure membrane fouling, *Water Res.*, 2012, **46**, 5531-5540.
43. R. K. Henderson, N. Subhi, A. Antony, S. J. Khan, K. R. Murphy, G. L. Leslie, V. Chen, R. M. Stuetz and P. Le-Clech, Evaluation of effluent organic matter fouling in ultrafiltration treatment using advanced organic characterisation techniques, *J. Membr. Sci.*, 2011, **382**, 50-59.
44. H. K. Shon, S. Vigneswaran, I. S. Kim, J. Cho and H. H. Ngo, Fouling of ultrafiltration membrane by effluent organic matter: A detailed characterization using different organic fractions in wastewater, *J. Membr. Sci.*, 2006, **278**, 232-238.
45. P. Le-Clech, V. Chen and T. A. G. Fane, Fouling in membrane bioreactors used in wastewater treatment, *J. Membr. Sci.*, 2006, **284**, 17-53.
46. F. L. Wang and V. V. Tarabara, Pore blocking mechanisms during early stages of membrane fouling by colloids, *J. Colloid Interface Sci.*, 2008, **328**, 464-469.
47. Q. L. Li and M. Elimelech, Organic fouling and chemical cleaning of nanofiltration membranes: Measurements and mechanisms, *Environ. Sci. Technol.*, 2004, **38**, 4683-4693.
48. M. Aslam, A. Charfi, G. Lesage, M. Heran and J. Kim, Membrane bioreactors for wastewater treatment: A review of mechanical cleaning by scouring agents to control membrane fouling, *Chem. Eng. J.*, 2017, **307**, 897-913.
49. C. S. Uyguner-Demirel, N. C. Birben and M. Bekbolet, Elucidation of background organic matter matrix effect on photocatalytic treatment of contaminants using TiO2: A review, *Catal. Today*, 2017, **284**, 202-214.
50. P. Mwaanga, E. R. Carraway and M. A. Schlautman, Preferential sorption of some natural organic matter fractions to titanium dioxide nanoparticles: influence of pH and ionic strength, *Environ. Monit. Assess.*, 2014, **186**, 8833-8844.
51. E. M. Carstea, J. Bridgeman, A. Baker and D. M. Reynolds, Fluorescence spectroscopy for wastewater monitoring: A review, *Water Res.*, 2016, **95**, 205-219.
52. R. K. Henderson, A. Baker, K. R. Murphy, A. Hambly, R. M. Stuetz and S. J. Khan, Fluorescence as a potential monitoring tool for recycled water systems: A review, *Water Res.*, 2009, **43**, 863-881.
53. C. Jacquin, G. Lesage, J. Traber, W. Pronk and M. Heran, Three-dimensional excitation and emission matrix fluorescence (3DEEM) for quick and pseudo-quantitative determination of protein- and humic-like substances in full-scale membrane bioreactor (MBR), *Water Res.*, 2017, **118**, 82-92.
54. W. Chen, P. Westerhoff, J. A. Leenheer and K. Booksh, Fluorescence Excitation−Emission Matrix Regional Integration to Quantify Spectra for Dissolved Organic Matter, *Environ. Sci. Technol.*, 2003, **37**, 5701-5710.

55. D. D. Phong and J. Hur, Non-catalytic and catalytic degradation of effluent dissolved organic matter under UVA-and UVC-irradiation tracked by advanced spectroscopic tools, *Water Res.*, 2016, **105**, 199-208.
56. R. X. Hao, H. Q. Ren, J. B. Li, Z. Z. Ma, H. W. Wan, X. Y. Zheng and S. Y. Cheng, Use of three-dimensional excitation and emission matrix fluorescence spectroscopy for predicting the disinfection by-product formation potential of reclaimed water, *Water Res.*, 2012, **46**, 5765-5776.
57. B. Guo, S. D. Snow, B. J. Starr, I. Xagoraraki and V. V. Tarabara, Photocatalytic inactivation of human adenovirus 40: Effect of dissolved organic matter and prefiltration, *Sep. Purif. Technol.*, 2018, **193**, 193-201.
58. S. Mozia, Photocatalytic membrane reactors (PMRs) in water and wastewater treatment. A review, *Sep. Purif. Technol.*, 2010, **73**, 71-91.
59. X. Zheng, Z. P. Shen, L. Shi, R. Cheng and D. H. Yuan, Photocatalytic Membrane Reactors (PMRs) in Water Treatment: Configurations and Influencing Factors, *Catalysts*, 2017, **7**, 30.
60. B. Pernet-coudrier, L. Clouzot, G. Varrault, M.-H. Tusseau-vuillemin, A. Verger and J.-M. Mouchel, Dissolved organic matter from treated effluent of a major wastewater treatment plant: Characterization and influence on copper toxicity, *Chemosphere*, 2008, **73**, 593-599.
61. D. Violleau, H. Essis-Tome, H. Habarou, J. P. Croué and M. Pontié, Fouling studies of a polyamide nanofiltration membrane by selected natural organic matter: an analytical approach, *Desalination*, 2005, **173**, 223-238.
62. X. Zheng, M. T. Khan and J.-P. Croué, Contribution of effluent organic matter (EfOM) to ultrafiltration (UF) membrane fouling: Isolation, characterization, and fouling effect of EfOM fractions, *Water Res.*, 2014, **65**, 414-424.
63. G. R. Aiken, D. M. McKnight, K. A. Thorn and E. M. Thurman, Isolation of hydrophilic organic acids from water using nonionic macroporous resins, *Org. Geochem.*, 1992, **18**, 567-573.
64. J. A. Leenheer, Systematic Approaches to Comprehensive Analyses of Natural Organic Matter, *Ann. Environ. Sci.*, 2009, **3**.
65. J. L. Weishaar, G. R. Aiken, B. A. Bergamaschi, M. S. Fram, R. Fujii and K. Mopper, Evaluation of Specific Ultraviolet Absorbance as an Indicator of the Chemical Composition and Reactivity of Dissolved Organic Carbon, *Environ. Sci. Technol.*, 2003, **37**, 4702-4708.
66. C. Goletz, M. Wagner, A. Grübel, W. Schmidt, N. Korf and P. Werner, Standardization of fluorescence excitation–emission-matrices in aquatic milieu, *Talanta*, 2011, **85**, 650-656.
67. M. Cho, H. Chung, W. Choi and J. Yoon, Linear correlation between inactivation of E. coli and OH radical concentration in TiO2 photocatalytic disinfection, *Water Res.*, 2004, **38**, 1069-1077.
68. J. R. Bolton and K. G. Linden, Standardization of methods for fluence (UV dose) determination in bench-scale UV experiments, *ASCE J. Environ. Eng.*, 2003, **129**, 209-215.
69. M. L. Quaranta, M. D. Mendes and A. A. MacKay, Similarities in effluent organic matter characteristics from Connecticut wastewater treatment plants, *Water Res.*, 2012, **46**, 284-294.
70. T. Masuda, S. Nakano and M. Kondo, Rate Constants for the Reactions of OH Radicals with the Enzyme Proteins as Determined by the p-Nitrosodimethylaniline Method, *Journal of Radiation Research*, 1973, **14**, 339-345.
71. C. L. Hawkins and M. J. Davies, Generation and propagation of radical reactions on proteins, *Biochim. Biophys. Acta*, 2001, **1504**, 196-219.
72. Y. Pi, J. Schumacher and M. Jekel, The Use of para-Chlorobenzoic Acid (pCBA) as an Ozone/Hydroxyl Radical Probe Compound, *Ozone: Science & Engineering*, 2005, **27**, 431-436.
73. I. Michael-Kordatou, C. Michael, X. Duan, X. He, D. D. Dionysiou, M. A. Mills and D. Fatta-Kassinos, Dissolved effluent organic matter: Characteristics and potential implications in wastewater treatment and reuse applications, *Water Res.*, 2015, **77**, 213-248.
74. A. Matilainen, E. T. Gjessing, T. Lahtinen, L. Hed, A. Bhatnagar and M. Sillanpaa, An overview of the methods used in the characterisation of natural organic matter (NOM) in relation to drinking water treatment, *Chemosphere*, 2011, **83**, 1431-1442.

75. J. K. Edzwald and J. E. Tobiason, Enhanced coagulation: Us requirements and a broader view, *Water Sci. Technol.*, 1999, **40**, 63-70.
76. M. Drosos, M. J. Ren and F. H. Frimmel, The effect of NOM to TiO2: interactions and photocatalytic behavior, *Appl. Catal. B-Environ.*, 2015, **165**, 328-334.
77. Y. Sun and J. J. Pignatello, Evidence for a surface dual hole-radical mechanism in the titanium dioxide photocatalytic oxidation of 2,4-D, *Environ. Sci. Technol.*, 1995, **29**, 2065-2072.
78. X. Huang, M. Leal and Q. Li, Degradation of natural organic matter by TiO2 photocatalytic oxidation and its effect on fouling of low-pressure membranes, *Water Res.*, 2008, **42**, 1142-1150.
79. E. Bouhabila, R. Ben Aim and H. Buisson, Fouling characterisation in membrane bioreactors, *Sep. Purif. Technol.*, 2001, **22-3**, 123-132.
80. S. L. Gora and S. A. Andrews, Adsorption of natural organic matter and disinfection byproduct precursors from surface water onto TiO2 nanoparticles: pH effects, isotherm modelling and implications for using TiO2 for drinking water treatment, *Chemosphere*, 2017, **174**, 363-370.
81. J. F. Budarz, A. Turolla, A. F. Piasecki, J. Y. Bottero, M. Antonelli and M. R. Wiesner, Influence of Aqueous Inorganic Anions on the Reactivity of Nanoparticles in TiO2 Photocatalysis, *Langmuir*, 2017, **33**, 2770-2779.
82. C. S. Turchi and D. F. Ollis, Photocatalytic degradation of organic water contaminants: Mechanisms involving hydroxyl radical attack, *J. Catal.*, 1990, **122**, 178-192.
83. T. E. Doll and F. H. Frimmel, Photocatalytic degradation of carbamazepine, clofibric acid and iomeprol with P25 and Hombikat UV100 in the presence of natural organic matter (NOM) and other organic water constituents, *Water Res.*, 2005, **39**, 403-411.
84. M. Long, J. Brame, F. Qin, J. Bao, Q. Li and P. J. Alvarez, Phosphate Changes Effect of Humic Acids on TiO2 Photocatalysis: From Inhibition to Mitigation of Electron-Hole Recombination, *Environ. Sci. Technol.*, 2017, **51**, 514-521.
85. B. J. Starr, V. V. Tarabara, M. Herrera-Robledo, M. Zhou, S. Roualdès and A. Ayral, Coating porous membranes with a photocatalyst: Comparison of LbL self-assembly and plasma-enhanced CVD techniques, *J. Membr. Sci.*, 2016, **514**, 340-349.